DOI: 10.61782/fa.2025.0628

FORUM ACUSTICUM
EURONOISE 2025

NUMERICAL ASSESSMENT OF A MODE DETECTION ARRAY FOR AZIMUTHAL DECOMPOSITION

Hugo Vincent* **Antonio Pereira** **Marc C. Jacob**

Ecole Centrale de Lyon, CNRS, Universite Claude Bernard Lyon 1, INSA Lyon, LMFA, UMR5509, 69130, Ecully, France

ABSTRACT

The efficiency of a mode detection array for azimuthal mode decomposition in turbofan nacelle experiments is numerically investigated by analyzing acoustic solutions computed using the commercial finite-element code ACTRANTM. First, irrotational inviscid mean flow fields are computed for sideline conditions, with and without an external flow at a Mach number of 0.2. Then, the upstream propagation of duct modes representing fan noise components is performed for three frequencies by solving the Möhring equation in the frequency domain using ACTRANTM. The acoustic solutions are interpolated to the microphone locations of the mode detection array. In all cases, the azimuthal structure of the interpolated data is obtained using Fourier transforms. It is compared to a reference one, determined by a duct mode decomposition of the full acoustic solution. The results provide guidelines for the analysis of ongoing experiments. They indicate that the detection antenna will be able to efficiently capture the azimuthal mode distributions, but not the radial structure. The procedure can be applied to design improved microphone arrays by defining judicious axial and radial positions for azimuthal and radial mode decompositions. Moreover, the approach can determine the optimum discretization for azimuthal mode decomposition.

Keywords: *aeroacoustics, duct mode, modal analysis*

**Corresponding author*: *hugo.vincent@ec-lyon.fr.*

1. INTRODUCTION

Aircraft produce noise that affects the health of people living near airports. Acoustic radiation originates mainly from the engine and, in particular, from the jet and the fan stage. With the development of Ultra-High Bypass Ratio (UHBR) engines, the noise produced in the fan stage has become the main noise contributor, as described in the recent review by Moreau [1]. The noise generated in the fan stage is characterized by tonal and broadband components. The tonal noise is produced at the Blade Passing Frequency (BPF) and its harmonics [2]. It is reduced by the use of acoustic liners [3], the optimization of which requires an in-depth knowledge of the acoustic field properties.

During their propagation in a turbofan intake, the acoustic waves reflect on the nacelle walls, leading to constructive and destructive interference at specific radial and azimuthal locations. As a result, the acoustic field can be decomposed into azimuthal and radial duct modes [4, 5]. The duct modes satisfy specific dispersion relations whose properties are used to determine key features of the acoustic field from in-duct experimental measurements [6–8].

The measurements are generally performed with wall-flush mounted microphones. The azimuthal structure of the acoustic field can easily be estimated from pressure measurements obtained on a microphone ring using Fourier transforms in the azimuthal direction. Computing the radial-mode amplitudes is more challenging since it is not possible to put microphones in the radial direction in a turbofan without significantly disturbing the flow. To the best of the authors' knowledge, Moore [6] was the first to describe a method for performing radial decomposition.

This method consists in projecting the acoustic field onto Bessel functions. Using this method, Moore [6] was able to decompose a synthetic field into azimuthal and radial modes. He also successfully applied the method to circumferential and radial measurements for a ventilation fan. Considering only measurements obtained in the azimuthal and axial directions, with rings and lines of microphones, and using the properties of the solutions of the convective wave equation, Enghardt *et al.* [7] were able to carry out an azimuthal and radial mode decomposition of the pressure fields measured in an axial-flow fan, using a method similar to the one introduced by Moore [6].

From measurements in the radial, azimuthal, and axial directions, it is possible to separate the upstream and downstream waves and to determine the amplitudes of the duct modes by applying procedures described by Rienstra [9]. However, in practice, such a full-mode decomposition cannot usually be performed because it requires microphones in the radial direction.

In the framework of the COMPANION (COMmon Platform and Advanced iNstrumentration readIness for ultra efficient propulsiON) project, pressure measurements obtained on a mode detection antenna will be analyzed to characterize the propagation of fan noise in a new-generation nacelle intake. The antenna is represented in figure 1. It is made of two rings and 4 axial lines linked to the azimuthal angles $\theta = 0, \pi/2, \pi$ and $3\pi/2$. All microphones are uniformly spaced and flush-mounted in the wall. A part of the nacelle intake is also depicted in figure 1. The geometry is non-axisymmetric and has a plane of symmetry.

The objective of the present work is to assess the capacity of the detection antenna to perform an azimuthal and radial decomposition. The study is conducted by analyzing pressure fields associated with fan noise propagating upstream through the nacelle intake. These pressure fields are simulated using the commercial finite element code ACTRANTM. Two flow configurations for sideline conditions and three frequencies are considered.

The remainder of this paper is organized as follows. Mean flow computations are documented in section 2. The numerical methods used for acoustic propagation calculations, as well as the pressure fields obtained, are described in section 3. A full mode breakdown is described in section 4. The capability of the antenna to perform azimuthal and radial decompositions is assessed in section 5. Concluding remarks are provided in section 6.

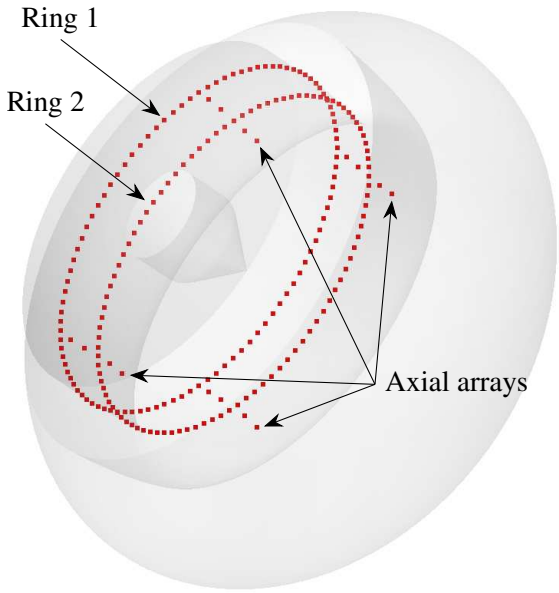

Figure 1. Representation of the inlet acoustic antenna composed of 2 rings and 4 axial lines; A part of the nacelle intake is displayed with transparency.

2. MEAN FLOW COMPUTATIONS

Two flow configurations associated with sideline conditions with and without an external flow at a Mach number of 0.2 are considered. Compressible irrotational inviscid mean flow fields are calculated using a potential flow solver implemented in ACTRAN. For that, an almost cylindrical computational domain is defined using the open-source software GMSH [10]. It is closed by an outlet surface normal to the flow direction located slightly downstream of the intersection between the rotor blades and the spinner. The rotor blades are not considered.

Mean pressure, density, and velocity fields are obtained by solving a generalised Laplace equation for the scalar potential using the finite element method. This equation is solved for an unstructured mesh composed of 9.4 million first-order triangles and tetrahedra generated using GMSH [10]. The element sizes were determined by a mesh sensitivity study, not described in this paper for the sake of brevity. The calculations required 28 GB of memory and less than one CPU hour. The mean flow fields were stored in all the mesh elements. They were used by ACTRANTM to solve the convected wave equation.

Cross-sections of the mean velocity fields obtained for $\mathrm{M_{ext}} = 0$ and $\mathrm{M_{ext}} = 0.2$ are represented in figures 2(a,b). For both cases, outside the nacelle, the levels are close to the exterior velocity associated with $\mathrm{M_{ext}} = 0$, as expected. Inside the geometry, they are higher and the mean velocity fields are nearly uniform, with velocity values around $165\,\mathrm{m/s}$. The strongest levels are found inside the geometry near the inlet lips. They are around $250\,\mathrm{m/s}$ for $\mathrm{M_{ext}} = 0$ and $200\,\mathrm{m/s}$ for $\mathrm{M_{ext}} = 0.2$. The flow near the inlet lips is thus more accelerated for $\mathrm{M_{ext}} = 0$ than for $\mathrm{M_{ext}} = 0.2$. These results are consistent with those reported by Doherty & Namgoong [11] and Xiong *et al.* [12].

3. ACOUSTIC PROPAGATION COMPUTATIONS

The acoustic propagation computations are carried out using ACTRANTM by solving a frequency domain formulation of the Möhring's equation [13], i.e. the convected wave equation for a non-uniform irrotational flow. Acoustic modes are injected slightly downstream of the intersection between the rotor blades and the spinner. Three arbitrarily chosen frequencies $f = 1000\,\mathrm{Hz}$, $3000\,\mathrm{Hz}$ and $5000\,\mathrm{Hz}$ are considered. They are associated with the Helmholtz numbers $\mathrm{He} = 2\pi f R/c_0 = 6, 18, 30$, where R is the outer duct radius and c_0 is the speed of sound in ambient medium. For each frequency, the propagation of all acoustic modes with a cut-off frequency below $3000\,\mathrm{Hz}$ is computed. The amplitude of the modes is set to $1\,\mathrm{Pa}$ at the injection plane. Thus, 16 modes are considered for $f = 1000\,\mathrm{Hz}$, whereas 126 modes are taken into account for $3000\,\mathrm{Hz}$ and $5000\,\mathrm{Hz}$.

The numerical methods used for the simulations are very similar to those recommended by Van Antwerpen *et al.* [14]. The computational domains are semi-elliptical and their size varies with frequency. Exploiting the planar symmetry of the nacelle intake, half-domain computations are performed using a fully automated strategy for decomposing the acoustic solutions into symmetric and anti-symmetric parts implemented in ACTRANTM. Acoustic meshes are generated using GMSH [10]. They are made of quadratic triangles and tetrahedra, and are refined so that each acoustic wavelength is discretized by at least four elements. The Perfectly matched layers (PMLs) described by Hu [15] are used at the boundaries considering non-uniform mean flow fields. Their thickness varies with frequency and is equal to $\lambda = c_0/f$. Six different meshes are thus considered. They contain between 710 000 and 7 200 000 nodes.

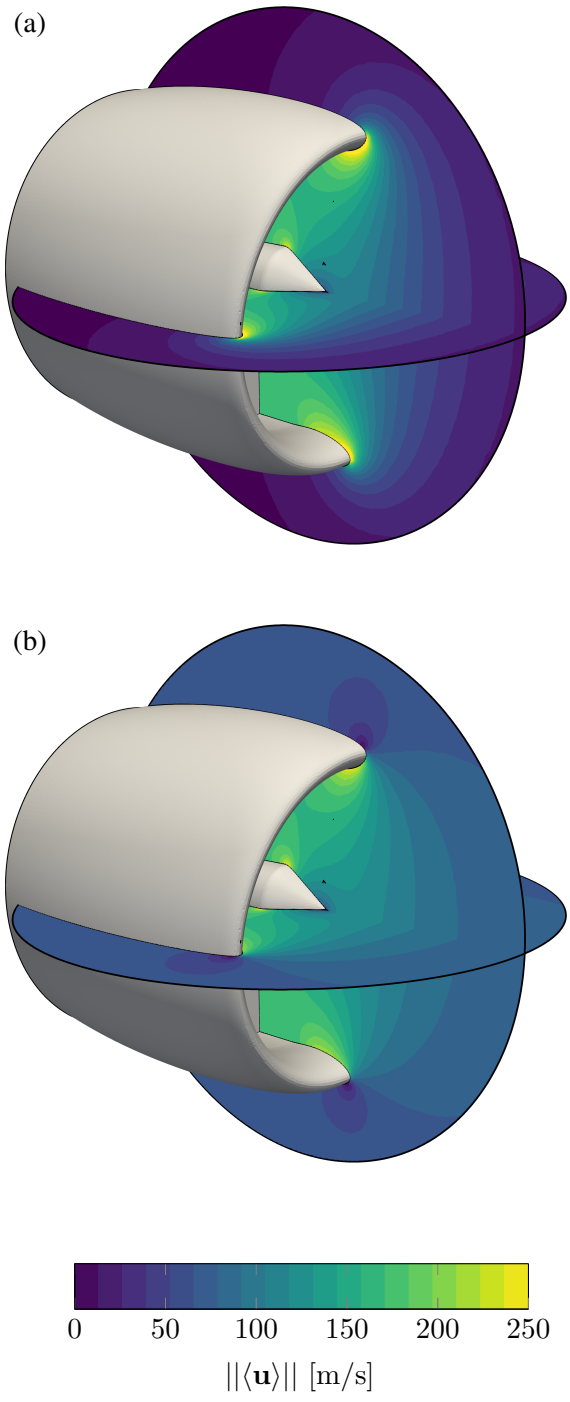

Figure 2. Magnitude of mean velocity vector on two longitudinal slices for sideline conditions and an external flow at (a) $\mathrm{M_{ext}} = 0$ and (b) $\mathrm{M_{ext}} = 0.2$.

For $f = 1000\,\text{Hz}$, the computations require around 8 GB of memory and less than one hour of CPU time. For $f = 5000\,\text{Hz}$, the simulations need approximately 200 GB of memory and 10 CPU hours. For each frequency and mode, the solutions have been stored on a full 3D mesh associated with the computational domain without the PML, on the microphone locations of the detection antenna, and on a cylindrical structured grid. The solutions for more than 500 modes were thus stored, constituting a database of approximately 700 GB.

The pressure fields obtained for the three frequencies 1000 Hz, 3000 Hz and 5000 Hz, for the two flow conditions with $\text{M}_{\text{ext}} = 0$ and $\text{M}_{\text{ext}} = 0.2$, for the plane mode, are represented in figures 3(a-f). In all cases, the propagation of acoustic waves through the inlet geometry and in the near field can be seen. The wavelengths are shorter for higher frequencies, and near the high velocity regions, as expected. For $f \geq 3000\,\text{Hz}$ in figures 3(b,c) and 3(e,f), the footprints of modes with radial orders $n \geq 0$ can be observed on the upstream boundaries of the domains.

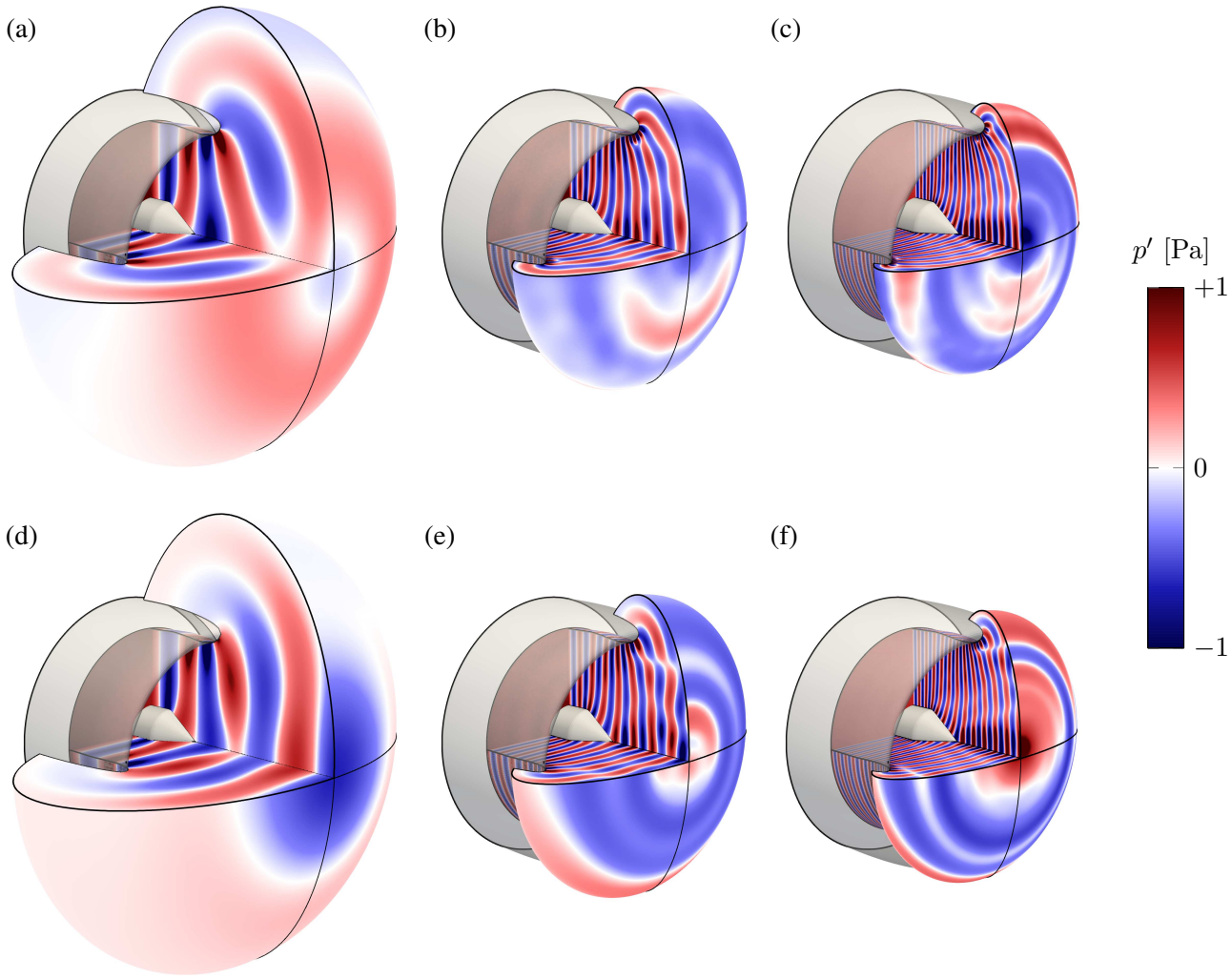

Figure 3. Representations of the real part of the pressure fields obtained for (a-c) $\text{M}_{\text{ext}} = 0$ and (d-f) $\text{M}_{\text{ext}} = 0.2$, and (a,d) $f = 1000\,\text{Hz}$, (b,e) $f = 3000\,\text{Hz}$ and (c,f) $f = 5000\,\text{Hz}$; three quarters of the computational domains without the PMLs are shown, and the geometry is displayed in gray with transparency.

4. DUCT-MODE DECOMPOSITION

The acoustic solutions are decomposed into upstream and downstream propagating azimuthal and radial modes by applying a procedure described by Rienstra [9]. The pressure fields satisfy equation (1), where $A_{m,n}$ and $B_{m,n}$ are respectively the amplitudes of the upstream and downstream propagating modes associated with the eigenfunctions for annular and circular duct sections $f_{m,n}$, and $k^+_{z_{m,n}}$ and $k^-_{z_{m,n}}$ are the associated axial wavenumbers, m and n are the azimuthal and radial orders, and i is the imaginary unit. The decomposition is performed for the duct-modes with azimuthal and radial orders between $m = 0$ and 4 and $n = 0$ and 4, using the complex pressure and axial velocity obtained on the structured grid previously mentioned. This grid is uniform and contains $N_r = 50$, $N_\theta = 64$, and $N_z = 60$ points in the radial, azimuthal, and axial directions. It extends radially from $r = 0$ up to the outer radius, and axially from $z = 0$ up to the end of the duct at $z \simeq 0.92R$. For each axial position, the amplitudes of the upstream and downstream propagating azimuthal and radial duct modes are estimated.

The contributions of the first five azimuthal modes to the sound pressure levels (SPL) of the upstream propagating fluctuations, obtained from the decomposition for the plane mode for $f = 3000\,\text{Hz}$, for $\text{M}_{\text{ext}} = 0$ and $\text{M}_{\text{ext}} = 0.2$ are represented as functions of the axial distance in figures 4(a,c). The axial positions of the two rings of the detection antenna are also depicted. In both cases, the dominant mode is axisymmetric, as expected for the plane mode. Upstream of the first ring for $z \gtrsim 0.25R$, strong levels are found for higher azimuthal orders $m = 1{-}4$, indicating that a proportion of the plane mode energy is redistributed on higher azimuthal modes during the propagation through the inlet. This was also the case in other studies [11, 12], and is certainly due to the non-axisymmetric geometry of the intake. The SPL of the axisymmetric mode for the first five radial modes in the flow conditions with $\text{M}_{\text{ext}} = 0$ and $\text{M}_{\text{ext}} = 0.2$, are displayed in figures 4(b,d). The plane mode is initially the mode with the highest energy content. This is not the case at the end of the duct, for $z \gtrsim 0.7r_0$, where the contributions of the radial modes with $n = 1 - 4$ are predominant, in agreement with the pressure fields in figures 3(b,e).

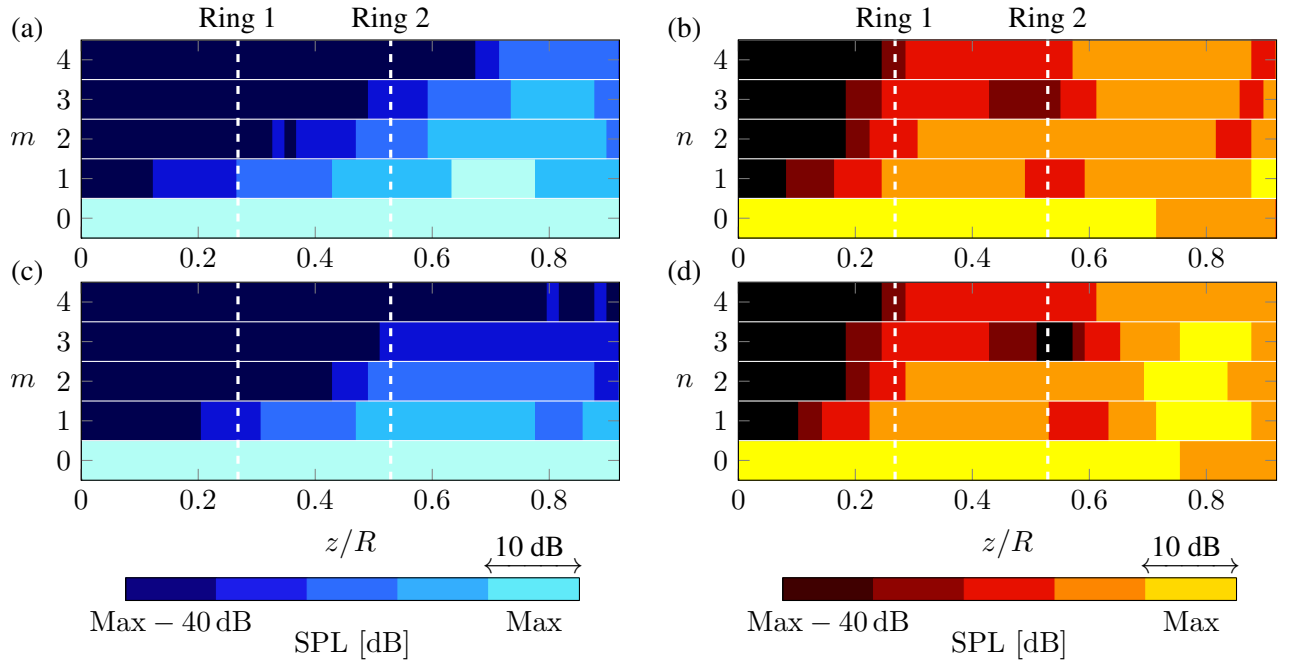

Figure 4. Sound pressure levels for the plane mode for $f = 3000\,\text{Hz}$ for (a,b) $\text{M}_{\text{ext}} = 0$ and (c,d) $\text{M}_{\text{ext}} = 0.2$, for upstream propagating (a,c) azimuthal modes and (b,d) axisymmetric radial modes ($m = 0$).

$$p\left(r,\theta,z\right)=\sum_{m=-\infty}^{\infty}\sum_{n=0}^{\infty}\left(A_{m,n}e^{ik_{z_{m,n}}^{+}z}+B_{m,n}e^{ik_{z_{m,n}}^{-}z}\right)f_{m,n}\left(r\right)e^{im\theta} \tag{1}$$

5. ASSESSMENT OF THE ANTENNA

To assess the capability of the antenna, only the complex pressure values obtained at the microphones of the detection antenna are analyzed in what follows. First, an azimuthal decomposition is performed by applying Fourier transforms to the pressure determined at the microphones of the two rings. The SPL obtained for the plane mode are represented as a function of the azimuthal order for the three frequencies for $\mathrm{M_{ext}} = 0$ in figures 5(a-c). They are displayed in red for Ring 1 and in blue for Ring 2. For both rings, the levels for the helical modes are stronger for higher frequencies, indicating that the redistribution of the plane mode energy on higher azimuthal modes is more important for these frequencies. Moreover, for $f = 5000\,\mathrm{Hz}$ in figure 5(c), the SPL associated with the first helical mode is approximately $15\,\mathrm{dB}$ higher than for the axisymmetric mode.

For all frequencies, the contributions of azimuthal modes with $m \geq 1$ are higher for Ring 2 than for Ring 1. They are therefore consistent with those determined along the duct axis, shown in figure 4(a). This indicates that the mode detection antenna can be useful for performing an azimuthal decomposition. Similar results, omitted here for clarity, are obtained for the other flow configuration with $\mathrm{M_{ext}} = 0.2$.

To investigate the ability of the mode detection antenna to perform a radial decomposition, the complex pressures obtained on the two rings and on the four axial lines are first arranged in a matrix $\mathbf{\Phi} \in \mathbb{C}^{K\times L}$, where L is the number of modes computed at a given frequency and K the total number of microphones in the antenna. Then, the modal coherence matrix [8, 16]

$$\mathbf{\Gamma} = \max_{1\leq i<j\leq L} \frac{|\langle \mathbf{\Phi}_i, \mathbf{\Phi}_j\rangle|}{\|\mathbf{\Phi}_i\|_2 \|\mathbf{\Phi}_j\|_2}, \tag{2}$$

where $\mathbf{\Phi}_i$ is the ith column of $\mathbf{\Phi}$, is computed for all cases. It quantifies the linear interdependence between two modes [17] and is therefore linked to the ability of the detection antenna to dissociate two modes.

The modal coherence values obtained for the first six cut-on axisymmetric modes for $f = 3000\,\mathrm{Hz}$ and $5000\,\mathrm{Hz}$ for $\mathrm{M_{ext}} = 0$ are presented in figures 6(a,b). In both cases, the values are equal to 1 along the diagonal since they are associated with the coherence of a mode with itself. They are also equal to 1 for the radial modes with $n \leq 3$, indicating that the footprints of these modes on the detection antenna are similar. This suggests that the antenna will not be able to separate these different radial modes. Overall, the coherence levels for $f = 5000\,\mathrm{Hz}$ in figure 6(a) are higher than those for $f = 3000\,\mathrm{Hz}$ in figure 6(b). This indicates that the capability of the

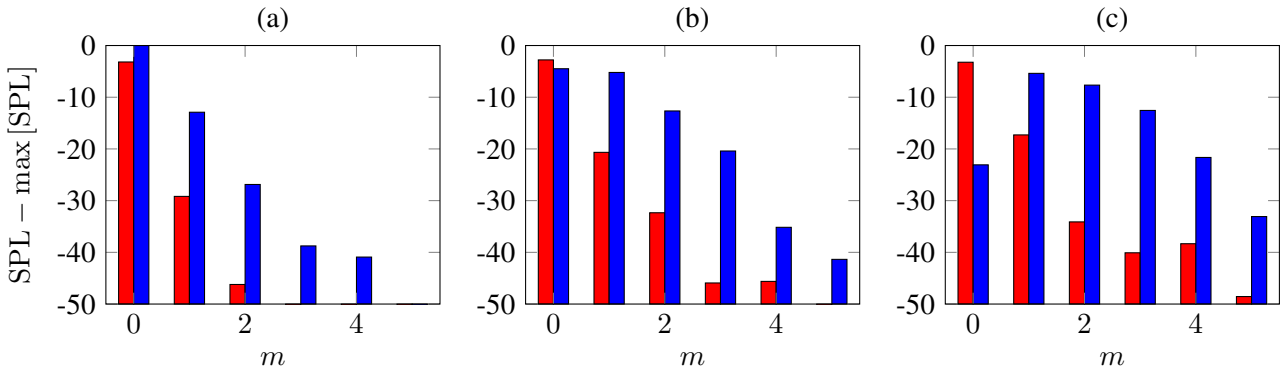

Figure 5. SPL for the plane mode as a function of the azimuthal order for (a) $f = 1000\,\mathrm{Hz}$, (b) $f = 3000\,\mathrm{Hz}$, (c) $f = 5000\,\mathrm{Hz}$ for $\mathrm{M_{ext}} = 0$, for the pressure obtained at the microphones of Ring 1 and Ring 2. The common SPL reference for the three plots is arbitrary.

antenna to distinguish two modes with the same azimuthal structure is reduced for a higher frequency.

The modal coherence levels obtained for 5000 Hz for $M_{ext} = 0.2$ are represented in figure 6(c). They are similar to those for $M_{ext} = 0$ in figure 6(a), suggesting that the ability of the antenna to separate two modes does not depend on the external flow Mach number.

A Tyler & Sofrin [2] mode linked to rotor-stator interaction is now considered. Its azimuthal order is $m = -4$. The coherence values obtained for the first five cut-on modes with $m = -4$ are displayed in figures 6(d-f). They exceed 0.5, suggesting that the detection antenna is not suitable for separating the radial modes of the Tyler & Sofrin mode under consideration. Moreover, the coherence levels for $m = -4$ are slightly lower than those for the plane mode in figures 6(a-c). The antenna therefore seems slightly better suited to separate modes with relatively high azimuthal modes.

6. CONCLUSIONS

The ability of a mode detection array for duct-mode decomposition in turbofan nacelle experiments is numerically investigated by analyzing acoustic solutions computed using the commercial code ACTRANTM. A full-mode breakdown is performed to obtain reference amplitudes for the upstream and downstream propagating azimuthal and radial modes. The detection antenna effectively captures azimuthal mode distributions. However, its capability to distinguish between modes with the same azimuthal structure remains limited. This provides guidelines for the analysis of future experimental measurements. In future work, it will be interesting to compare the results with solutions obtained using analytical models [18] or a Green's function discretization technique [19]. It could also be interesting to apply an inverse method [20] to determine the modal amplitudes.

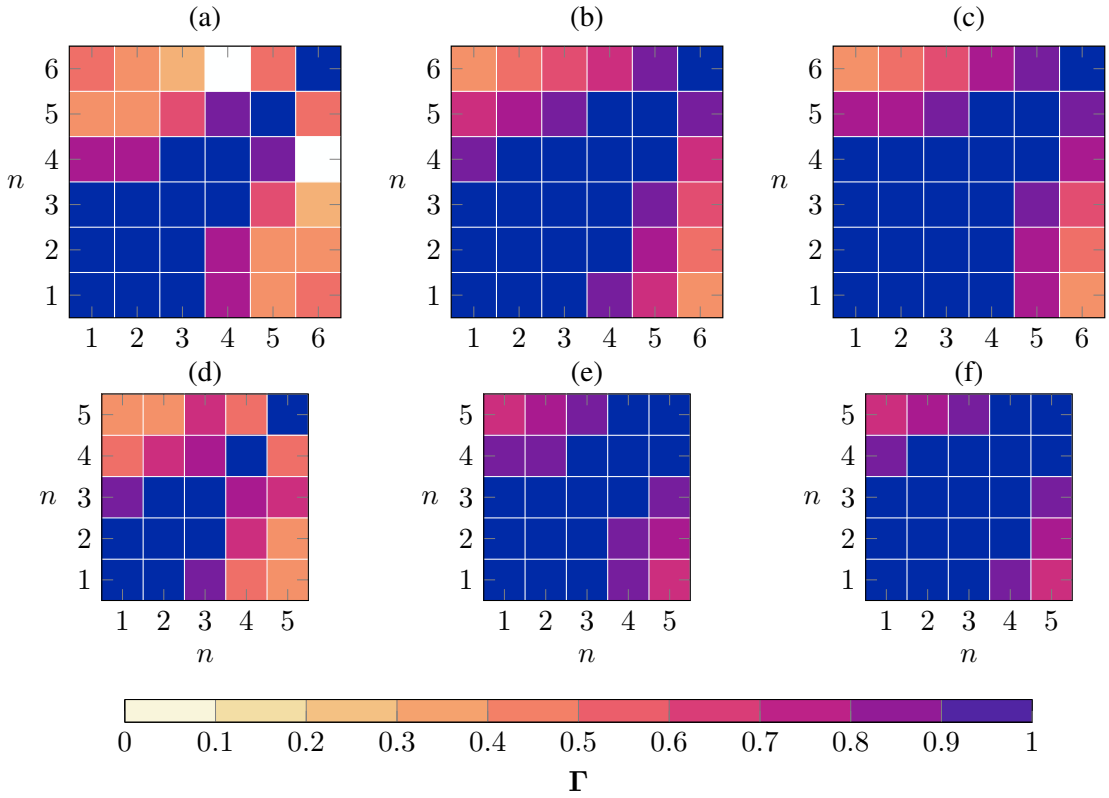

Figure 6. Modal coherence for (a,d) $f = 3000$ Hz and (b,e) $f = 5000$ Hz for $M_{ext} = 0$, and (c,f) $f = 5000$ Hz for $M_{ext} = 0.2$, for (a-c) the first six axisymmetric modes ($m = 0$) and (d-f) the first five modes with $m = -4$, which is the azimuthal order of a Tyler & Sofrin mode.

7. ACKNOWLEDGMENTS

This research has been performed in the frame of the project COMPANION (COMmon Platform and Advanced iNstrumentration readIness for ultra efficient propulsiON), which is funded by the European Union Clean Aviation Joint Undertaking program, under grant agreement No. 101140627. The authors gratefully acknowledge Emmanuel Julliard (Airbus) for useful discussions. This work was granted access to the HPC resources of PMCS2I (Pôle de Modélisation et de Calcul en Sciences de l'Ingénieur de l'Information) of Ecole Centrale de Lyon. It was performed within the framework of the LABEX CeLyA (ANR-10-LABX-0060) of Université de Lyon, within the program *Investissements d'Avenir* (ANR-16-IDEX-0005) operated by the French National Research Agency (ANR).

8. REFERENCES

[1] S. Moreau, "Turbomachinery noise predictions: present and future," *Acoustics*, vol. 1, no. 1, 2019.

[2] J. M. Tyler and T. G. Sofrin, "Axial flow compressor noise studies," *SAE Technical Paper 620532*, 1962.

[3] M. G. Jones, W. R. Watson, D. M. Nark, B. M. Howerton, and M. C. Brown, "A review of acoustic liner experimental characterization at NASA Langley," *NASA Technical Report 2020-220583*, 2020.

[4] C. Morfey, "Rotating pressure patterns in ducts: Their generation and transmission," *Journal of Sound and Vibration*, vol. 1, no. 1, 1964.

[5] S. W. Rienstra and A. Hirschberg, *An introduction to acoustics*. Eindhoven University of Technology, 2004.

[6] C. Moore, "Measurement of radial and circumferential modes in annular and circular fan ducts," *Journal of Sound and Vibration*, vol. 62, no. 2, 1979.

[7] L. Enghardt, Y. Zhang, and W. Neise, "Experimental verification of a radial mode analysis technique using wall-flush mounted sensors," *Meeting of the Acoustical Society of America*, 1999.

[8] A. Pereira, A. Finez, Q. Leclere, E. Salze, and P. Souchotte, "Modal identification of a small-scale ducted fan," *AIAA Paper 2016-3063*, 2016.

[9] S. W. Rienstra, "Fundamentals of duct acoustics," *Von Karman Institute Lecture Notes*, vol. 589, 2015.

[10] C. Geuzaine and J.-F. Remacle, "Gmsh: A 3-D finite element mesh generator with built-in pre- and post-processing facilities," *International Journal for Numerical Methods in Engineering*, vol. 79, no. 11, 2009.

[11] M. Doherty and H. Namgoong, "Impact of turbofan intake distortion on fan noise propagation and generation," *AIAA Paper*, 2016.

[12] L. Xiong, R. Sugimoto, and E. Quaranta, "Effects of turbofan engine intake droop and length on fan tone noise," *AIAA Paper 2019-2581*, 2019.

[13] W. Mohring, "A well posed acoustic analogy based on a moving acoustic medium," *Aeroacoustic Workshop SWING*, 1999.

[14] B. V. Antwerpen, Y. Detandt, D. Copiello, E. Rosseel, and E. Gaudry, "Performance improvements and new solution strategies of Actran/TM for nacelle simulations," *AIAA Paper 2014-2315*, 2014.

[15] F. Q. Hu, "A perfectly matched layer absorbing boundary condition for linearized euler equations with a non-uniform mean flow," *Journal of Computational Physics*, vol. 208, no. 2, 2005.

[16] M. Behn, R. Kisler, and U. Tapken, "Efficient azimuthal mode analysis using compressed sensing," *AIAA Paper 2016–3038*, 2016.

[17] F. O. Castres and P. F. Joseph, "Experimental investigation of an inversion technique for the determination of broadband duct mode amplitudes by the use of near-field sensor arrays," *The Journal of the Acoustical Society of America*, vol. 122, no. 2, 2007.

[18] D. Lewis, J. de Laborderie, M. Sanjosé, S. Moreau, M. C. Jacob, and V. Masson, "Parametric study on state-of-the-art analytical models for fan broadband interaction noise predictions," *Journal of Sound and Vibration*, vol. 514, 2021.

[19] D. Casalino, M. Roger, and M. C. Jacob, "Prediction of sound propagation in ducted potential flows using Green's function discretization," *AIAA Journal*, vol. 42, no. 4, 2004.

[20] A. Pereira and M. C. Jacob, "Modal analysis of in-duct fan broadband noise via an iterative bayesian inverse approach," *Journal of Sound and Vibration*, vol. 520, 2022.